Microelectronic Engineering 148 (2015) 59–63

Contents lists available at ScienceDirect

Microelectronic Engineering

journal homepage: www.elsevier.com/locate/mee

The optical and electrical properties of gallium-doped ZnO thin film with post-annealing processes of various atmospheres

Chien-Sheng Huang *, Ching-Chun Liu

Department of Electronic Engineering, National Yunlin University of Science and Technology, Yunlin 64002, Taiwan

ARTICLE INFO

Article history:
Received 15 June 2015
Received in revised form 5 August 2015
Accepted 6 August 2015
Available online 7 August 2015

Keywords:
Ga-doped
ZnO
TCO
Annealing

ABSTRACT

In this study, the GZO thin film were deposited with different RF powers and plasma gas of pure argon, 5% oxygen to argon ratio, and 10% oxygen argon ratio. After that, post-thermal annealing processes were performed at the temperature of 300 °C to 500 °C under vacuum, nitrogen, or acetylene ambient. The carrier concentrations and mobility exhibited different dependencies on these fabrication parameters, and that would reverse the conductivity order of as-sputtered samples. As a result, the carbon atom in the acetylene dissolved into the GZO thin film during post-thermal annealing and benefited the free carrier concentrations as another effective donor besides the gallium. The optical bandgap increased due to the increasing free carrier concentration, and made transparency still above 80%.

1. Introduction

Due to both their good conductivity and transparency in the optical visible range (VIS), transparent conducting oxides (TCOs) are widely used in many opto-electronic devices, such as solar cells, liquid crystal displays (LCDs), and light emitting diodes (LEDs) or organic electroluminescence device (OLEDs). In modern technology, tin doped In_2O_3 (ITO) is the most extensively utilized TCO thin film. There are also other kinds of them, e.g., antimony or fluorine doped SnO_2 (ATO and FTO), Al doped ZnO (AZO), and Ga doped ZnO (GZO). They all own the feature of binary or ternary compounds, with one or two metallic atoms. It is usually difficult for intrinsic stoichiometric oxides to attain remarkable combination of conductivity and transparency. However, by a non-stoichiometric composition or by introducing an appropriate dopant, CdO thin films were first found to possess such characteristics [1], and later ZnO, SnO_2, In_2O_3 and their alloys were also recognized as TCOs [2]. Since Indium is a rare substance, researches on AZO or GZO thin films as alternatives are attractive and practical [3–6]. Moreover, they are also non-toxic and abundant, friendly to the environment in the manufacturing process.

There are many methods for the fabrication of AZO or GZO thin films, such as electron beam evaporation [7], ion planting [8], sol–gel methods [9], spray pyrolysis [10], and magnetron sputtering [11–14]. The characteristics of as-made thin films are different according to the fabrication methods, and magnetron sputtering is the major one for the commercial production. The reason is the high reproducibility of uniform coatings over large areas [15]. Nevertheless, the conditions of the sputtering strongly influence the structural, electrical, and optical properties of as-deposited AZO and GZO films [4]. The sputtering deposition parameters include the total pressure and flow rates of used gases in the chamber, the distance between the target and substrate, and even the source power used. For ZnO, although crystalline (002) is the primary thin film growth direction due to its lowest surface free energy, the competition of other directions exists such as (100), (101), (102), and (110). The partial gas pressure ratio of oxygen to argon would affect the final surface primary direction and morphology [16,17]. In short, it is related to the plasma constitutions and the nuclei formation on the substrate surface. Compared with the radius of Al^{+3} cation (0.053 nm), that of Ga^{+3} cation (0.062 nm) is closer to that of Zn^{+2} (0.060 nm), and hence the defects of GZO thin film would reduce. Post-thermal annealing processes were also explored to improve the electrical property of GZO, and the annealing temperatures were the major parameters to be determined under vacuum, oxygen, or nitrogen ambient [18]. Not only in the Ga-doped thin film was the post-thermal annealing a necessary process, but also in the Ga-doped nanosheets or nanorods to improve the electrical and optical properties [19–22].

In this study, Ga-doped ZnO films were deposited on the glass substrate by an RF-sputter with a 3 wt.%Ga_2O_3–ZnO target. The deposition parameters consisted of the RF source power, the gas flow rate ratio of argon and oxygen during deposition. The post-thermal annealing conditions were categorized as the vacuum, nitrogen ambient, and acetylene ambient. The physical properties of each GZO thin film were investigated by low scattering angle X-ray diffraction (XRD), X-ray photoelectron spectra (XPS), scanning electron microscope (SEM), and atomic force microscopy (AFM). The electrical properties were measured by the Hall effect measurement, and optical properties measured by the UV–VIS spectrum. It was found the underlying physical properties were

* Corresponding author.
E-mail address: kenttyhuang@gmail.com (C.-S. Huang).

http://dx.doi.org/10.1016/j.mee.2015.08.002
0167-9317/

relative to the explanation of the electrical and optical properties. The post-annealing by acetylene ambient other than vacuum or nitrogen showed the best performance.

2. Material and methods

In this experiment, all the substrates are B270 optical glass. The RF sputtering target is ZnO:Ga_2O_3 (97/3 wt.%) with three inches diameter. The RF source power could be 110 W, 120 W, 130 W, 140 W and 150 W, respectively. The chamber were vacuumed to a base pressure of 5×10^{-6} Torr, and the substrate holder was not heated. For lighting plasma, argon and oxygen gases were used, and the total gas flow rate was kept 20 sccm, with the working pressure upwards to 20 mTorr. There were three various compositions of argon and oxygen plasma gases: pure argon, 5% oxygen to argon, and 10% oxygen to argon, respectively. Since the deposition rates were different for these three gases compositions, the thickness of such-deposited sample was controlled differently by the required sputtering times.

The post-thermal annealing processes were performed by a quartz tube furnace, which would be vacuumed to a pressure of 2×10^{-2} Torr by a rotary pump, in the meantime kept at a temperature parameter of 300 °C, 400 °C, 450 °C, and 500 °C, respectively. For nitrogen or acetylene ambient annealing, the flow of corresponding gas would let the pressure inside the tube upwards to 3.5 Torr.

The crystalline structure of samples was investigated by the low angle X-ray diffraction (Bede D1 HR-XRD) with the incident angle of 1°, scanning speed of 3°/min, and ranges of 20° to 80°. The compositions of GZO before and after annealing were measured by XPS (Thermo K-Alpha).

The surface morphology and grain size of samples were examined by the FE-SEM (JEOL JSM-7500 F), and the surface roughness by the AFM.

The electrical properties of samples were characterized by the Hall measurement (Ecopia), and the optical properties of samples by the absorption and transmission spectra of UV–VIS spectrometer.

3. Results and discussion

Fig. 1 showed the variation of the resistivity ρ and conductivity σ ($\sigma = 1/\rho$) of as-deposited GZO thin film with pure argon plasma and without post-annealing treatment by various RF powers of 110 W, 120 W, 130 W, 140 W, and 150 W, respectively. The resistivity decreased as the RF power increased, as explained by two reasons in the former literature that high RF power prevented the surface oxidation and helped to form a dense and defect free film [23].

The deposition rate for various gas plasma compositions with the RF power of 140 W was shown in Fig. 2(a), and the corresponding

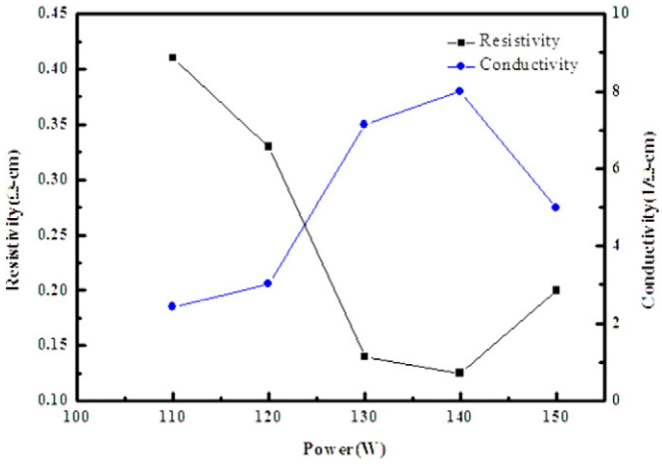

Fig. 1. Variation of the resistivity and conductivity by various RF power with pure argon plasma and without post-annealing.

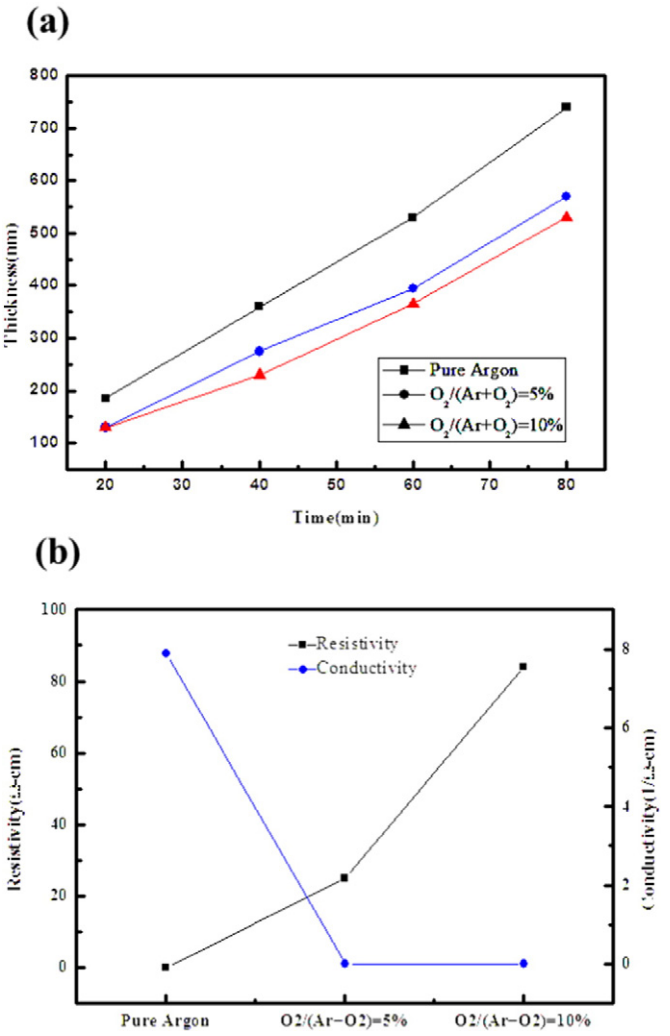

Fig. 2. (a) The deposition rate of various gas plasma compositions with 140 W RF power, (b) the resistivity and conductivity of 360 nm thickness thin film.

resistivity of as-deposited 360 nm thickness GZO thin film shown in Fig. 2(b). The deposition rate of the pure argon plasma was larger, and with the increasing oxygen ratio, the deposition rate was reducing. The reason is that argon is inert gas and has larger momentum than oxygen of reaction [24]. Moreover, the resistivity of as-deposited thin film also increased with the increasing oxygen ratio. The conductivity comes from the free carrier concentration multiplying the free carrier mobility in the GZO thin film. Oxygen vacancies contribute partially to the free carrier concentration. When the GZO thin film was sputtered in an oxygen rich circumstance, the oxygen vacancy declined and hence the free carrier concentrations decreased, resulting in the decrease of conductivity (the increase of the resistivity).

Fig. 3(a)–(d) showed the effects of post-thermal annealing temperature under nitrogen ambient on the free carrier, free carrier mobility, the resistivity and the relative resistivity ratio, respectively. The carrier concentration increased as the annealing temperature increased. However, while the annealing temperature was higher than 400 °C, the carrier concentration would decrease. The free carrier mobility was determined by the crystalline property and the grain size. The XRD and SEM results gave the positive trend with the increasing annealing temperature, i.e., larger grain size. Moreover, by comparison Fig. 3(c) with the as-sputtered samples shown in Fig. 2(b), the post-thermal annealing would reverse the order of conductivity with pure argon the worst. Fig. 3(d) showed the relative resistivity ratio Z ($Z = \rho_{before\_annealing} / \rho_{after\_annealing}$) to indicate the improvement of

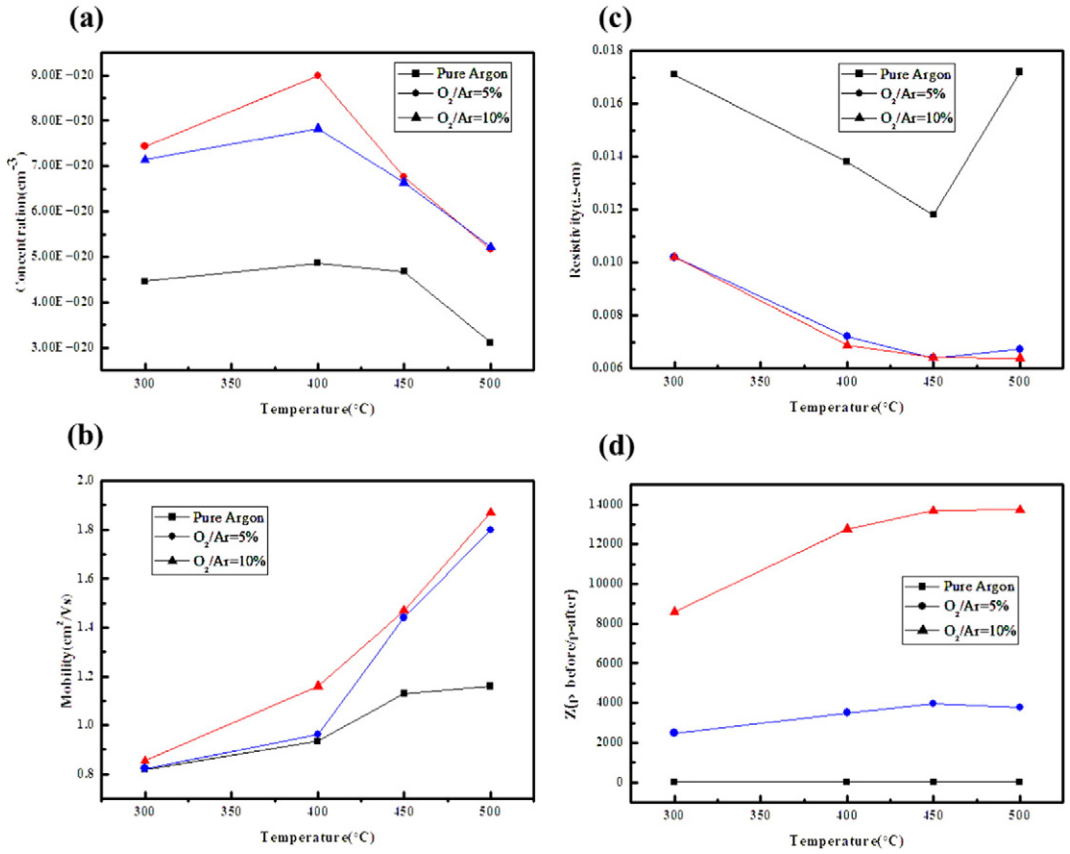

Fig. 3. With nitrogen ambient post-annealing, the variations of (a) free carrier concentration, (b) mobility, (c) the resistivity, and (d) the relative resistivity ratio to the annealing temperatures.

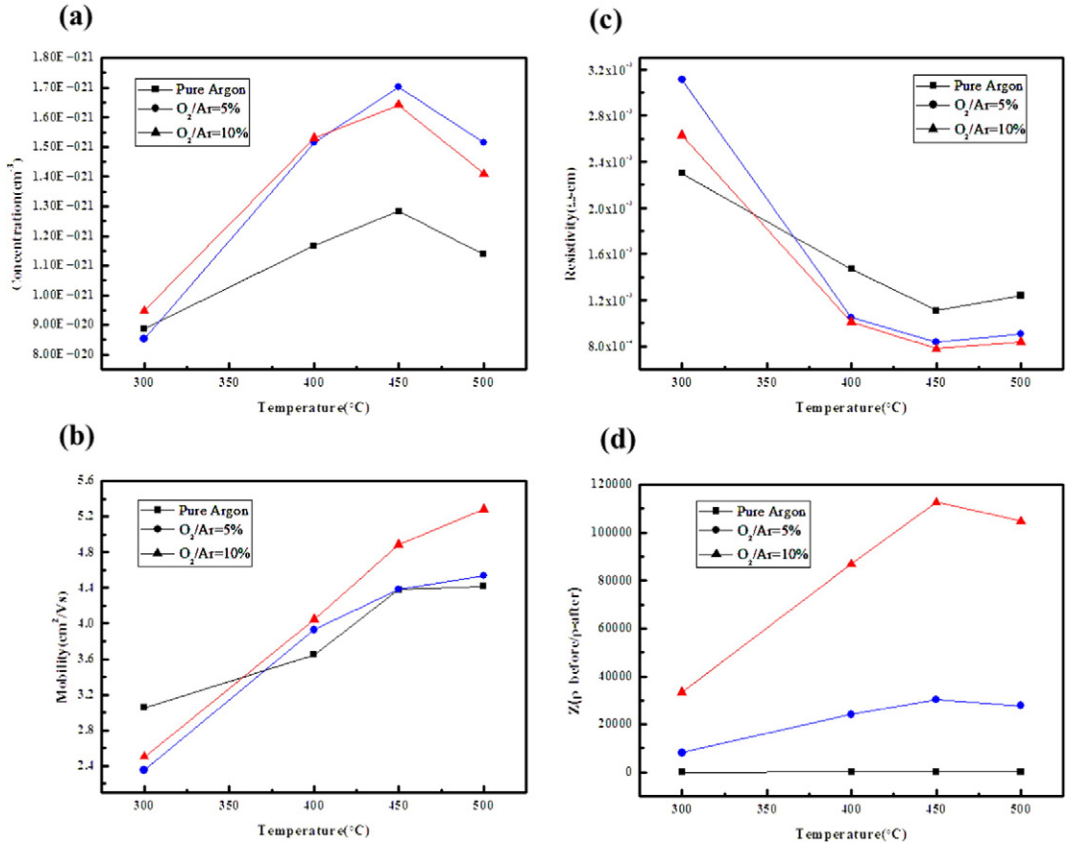

Fig. 4. With acetylene ambient post-annealing, the variations of (a) free carrier concentration, (b) mobility, (c) the resistivity, and (d) the relative resistivity ratio to the annealing temperatures.

the post-annealing on the resistivity [25]. The annealing temperature above 400 °C would reach saturation due to the decrease in the free carrier concentration.

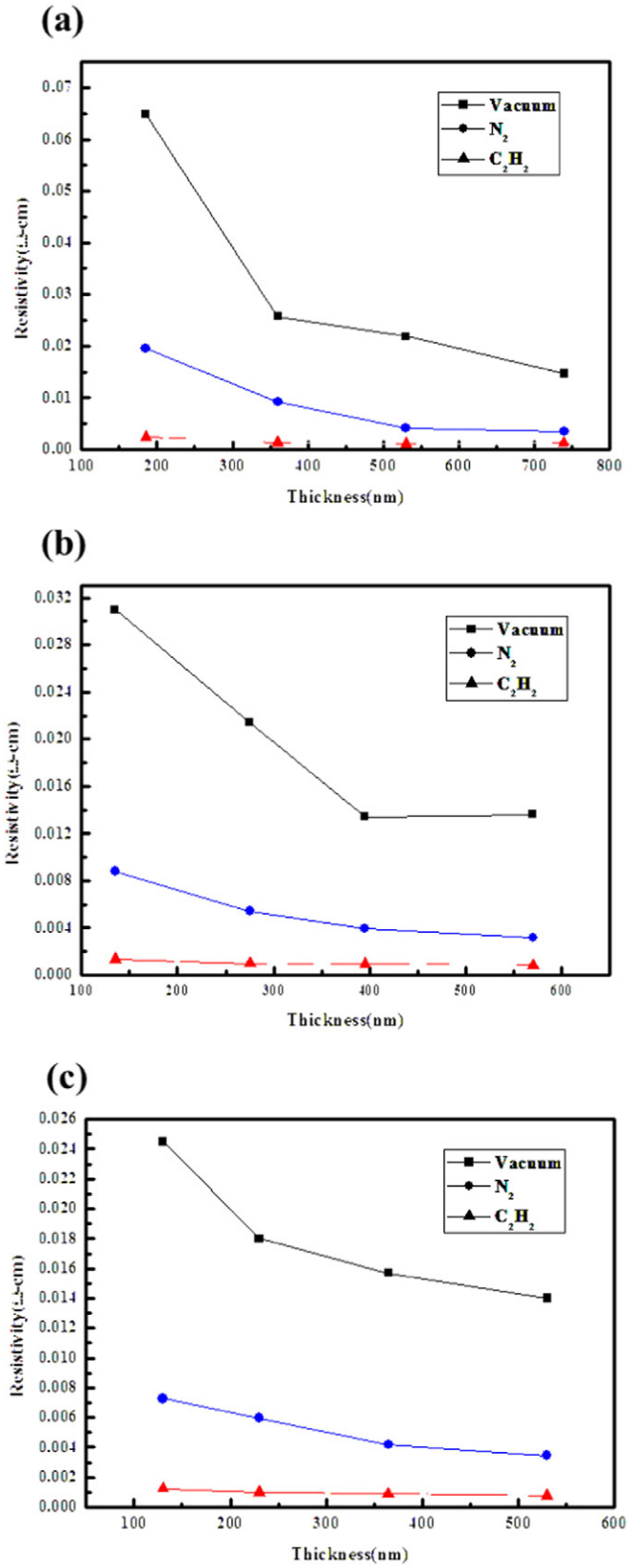

Fig. 5. The variations of resistivity to the film thickness under various post-annealing ambient and made of various plasma gas compositions of (a) pure argon, (b) 5% oxygen ratio, and (c) 10% oxygen ratio.

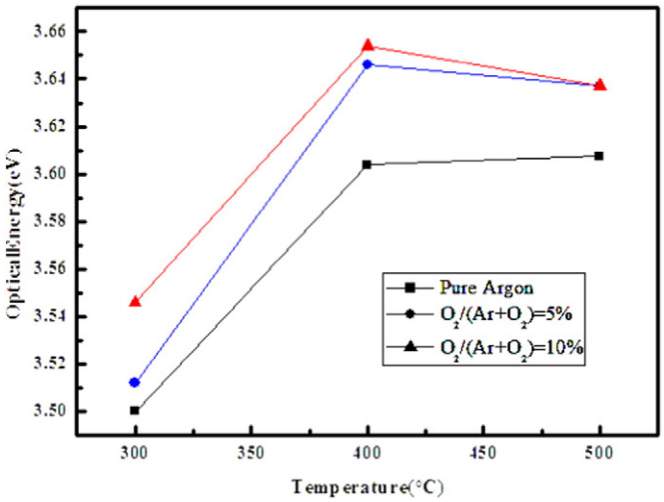

Fig. 6. The optical bandgap of as-deposited film under acetylene post-annealing ambient.

Fig. 4(a)–(d) showed the effects of post-thermal annealing temperature under acetylene ambient on the free carrier, free carrier mobility, the resistivity and the relative resistivity ratio, respectively. As discussed above, the relative resistivity ratio Z represented the improvement of the post-annealing. For the acetylene ambient, the order of magnitude was much larger than that of the nitrogen ambient. The carbon atom provided by the acetylene dissolved into the GZO thin film and acted as effect donors to increase the carrier concentration.

Fig. 5(a)–(c) showed the variations of resistivity to the film thickness under various post-annealing ambient and made of various plasma gas compositions of pure argon, 5% oxygen ratio, and 10% oxygen ratio, respectively. As the film thickness above 400 nm, the improvement on the resistivity was limited.

The optical bandgap variation to the annealing temperature under acetylene was shown in Fig. 6. The increase in the optical bandgap resulted in the lowering effect of the absorption onset wavelength of the GZO thin film, which remained transparent in the optical vision range. The increasing free carrier concentration could explain the increase on the optical bandgap. The measured UV–VIS spectra showed the transparency still above 80% in the optical vision range.

4. Conclusions

In summary, GZO thin film were successfully deposited under various plasma gas compositions, and annealed at different temperature under vacuum, nitrogen, or acetylene ambient. The annealing temperatures of 400 °C to 450 °C had the best improvement on the resistivity, and the acetylene annealing ambient exhibited tremendous effects than nitrogen. Moreover, the increase in the free carrier concentration contributes to the increasing of the optical bandgap, and hence benefited on the transparency.

References

[1] K. Baedeker, Ann. Phys. (Leipzig) 22 (1907) 749–766.
[2] G. Haacke, Annu. Rev. Mater. Sci. 7 (1977) 73–93.
[3] A. Tanaka, M. Hirata, Y. Kiyohara, M. Nakano, K. Omae, M. Shiratani, K. Koga, Thin Solid Films 518 (2010) 2934–2936.
[4] J. Jia, A. Takasaki, N. Oka, Y. Shigesato, J. Appl. Phys. 112 (2012) 013718.
[5] S.J. Young, Y.H. Liu, C.H. Hsiao, S.J. Chang, B.C. Wang, T.H. Kao, K.S. Tsai, S.L. Wu, IEEE Transactions on Nanotechnology 13 (2014) 238–244.
[6] Junjun Jia, Aya Yoshimura, Yukihiro Kagoya, Nobuto Oka, Yuzo Shigesato, Thin Solid Films 559 (2014) 69–77.
[7] D.R. Sahu, S.-Y. Lin, J.-L. Huang, Microelectron. J. 38 (2007) 245.
[8] T. Yamada, H. Makino, N. Yamamoto, T. Yamamoto, J. Appl. Phys. 107 (2010) 123534.
[9] H. Karaagac, E. Yengel, M.S. Islam, J. Alloys Compd. 521 (2012) 155.

[10] P. Nunes, A. Malik, B. Fernandes, E. Fortunato, P. Vilarinho, R. Martins, Vacuum 52 (1999) 45.
[11] M. Kon, P.K. Song, Y. Shigesato, P. Frach, A. Mizukami, K. Suzuki, Jpn. J. Appl. Phys. 41 (2002) 814.
[12] R. Martins, E. Fortunato, P. Nunes, I. Ferreira, A. Marques, M. Bender, N. Katsarakis, V. Cimalla, G. Kiriakidis, J. Appl. Phys. 96 (2004) 1398.
[13] K. Hirohata, Y. Nishi, N. Tsukamoto, N. Oka, Y. Sato, I. Yamamoto, Y. Shigesato, Thin Solid Films 518 (2010) 2980.
[14] Y. Nishi, K. Hirohata, N. Tsukamoto, Y. Sato, N. Oka, Y. Shigesato, J. Vac. Sci. Technol. A 28 (2010) 890.
[15] N. Ito, N. Oka, Y. Sato, Y. Shigesato, Jpn. J. Appl. Phys. 49 (2010) 071103.
[16] W.T. Lim, C.H. Lee, Thin Solid Films 353 (1999) 12–15.
[17] F.K. Shan, G.X. Liu, W.J. Lee, B.C. Shin, S.C. Kim, J. Electroceram. 17 (2006) 287–292.
[18] G. Gonçalves, E. Elangovan, P. Barquinha, L. Pereira, R. Martins, E. Fortunato, Thin Solid Films 515 (2007) 8562–8566.
[19] C.C. Yang, Y.K. Su, C.H. Hsiao, S.J. Young, T.H. Kao, M.Y. Chung, Y.C. Huang, B.C. Wang, S.L. Wu, IEEE Photon. Technol. Lett. 26 (2014) 1317–1320.
[20] S.J. Chang, B.G. Duan, C.H. Hsiao, C.W. Liu, S.J. Young, IEEE Photon. Technol. Lett. 26 (2014) 66–69.
[21] C.H. Hsiao, C.S. Huang, S.J. Young, S.J. Chang, J.J. Guo, C.W. Liu, S.J. Chang, J. Nanosci. Nanotechnol. 13 (2013) 8320–8324.
[22] C.H. Hsiao, C.S. Huang, S.J. Young, S.J. Chang, J.J. Guo, C.W. Liu, T.Y. Yang, IEEE Trans. Electron Devices 60 (2013) 1905–1910.
[23] J.F. Chang, H.L. Wang, M.H. Hon, J. Cryst. Growth 211 (2000) 93–97.
[24] C.H. Ahn, Y.Y. Kim, S.W. Kang, B.H. Kong, S.K. Mohanta, H.K. Cho, J.H. Kim, H.S. Lee, J. Mater. Sci. Mater. Electron. 19 (2008) 744–748.
[25] V. Khranovskyy, U. Grossnerb, V. Lazorenkoa, G. Lashkareva, B.G. Svenssonb, R. Yakimovac, Superlattice. Microst. 42 (2007) 379–386.